Spin Peltier Effect: Controlling Heat Through Electron Spins

KEN-ICHI UCHIDA
NATIONAL INSTITUTE FOR MATERIALS SCIENCE

Interaction between spin and heat currents is actively studied in the field of spin caloritronics from the viewpoints of both fundamental physics and applications. The phenomenon of spin-current generation due to a heat current is called the spin Seebeck effect and is garnering attention as a new thermoelectric conversion principle. Its reciprocal effect—the spin Peltier effect—is a phenomenon where the heat current is generated by a spin current. In recent years, we successfully observed the temperature change caused by the spin Peltier effect by using the lock-in thermography method, which has mainly been used for semiconductor device analyses, and demonstrated a unique temperature distribution induced by the spin current. In this article, we review our recent studies on spin caloritronics by focusing particularly on thermal imaging measurements of the spin Peltier effect.

INTRODUCTION

The interaction of spin and heat gives rise to various physical phenomena and new functions in magnetic materials. Specifically, with the discovery of the spin Seebeck effect (SSE) [1-4] in which a temperature gradient applied to a magnetic material generates a spin current (a flow of spin-angular momentum) [5], a field called "spin caloritronics" [6,7] that fuses spintronics and thermal transport has progressed rapidly. The name spin caloritronics was first proposed by Hatami et al. [8] in 2007 and quickly spread worldwide as studies on the SSE became popular.

Early studies on spin caloritronics mainly focused on phenomena that generate a spin current from a heat current, such as the SSE, toward the development of versatile thermoelectric generators [9,10]. In contrast, there are many heat-generation phenomena that use a spin current or magnetic field as input, e.g., the spin Peltier effect (SPE) [11-17], which is the reciprocal of the SSE (Fig. 1); the anisotropic magneto-Peltier effect [18], in which the charge-to-heat current conversion efficiency depends on the angle between the charge current and magnetization in a ferromagnet; the Ettingshausen effect [19-21], in which a heat current is generated in the direction perpendicular to both the applied charge current and magnetic field or magnetization; and the magnetocaloric effect, in which the temperature of a magnetic material changes with the magnetic field [22-24]. Recently, we successfully observed the thermal response from these phenomena by means of active infrared emission microscopy called lock-in thermography (LIT) [25-27], and demonstrated thermal control functions that cannot

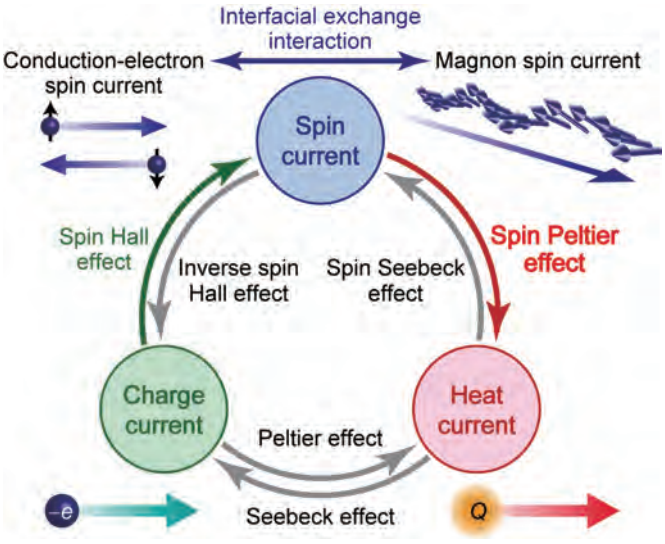

Fig. 1: Physical phenomena enabling the conversion between spin, charge, and heat currents [17]. A spin current is typically carried by conduction electrons and magnons; the conduction-electron spin currents can be converted into the magnon spin currents, and vice versa, via the exchange interaction at the paramagnet/ferro- or ferrimagnet interface.

be actualized without magnetic materials and spintronics. This article outlines our LIT experiments for measuring the SPE and shows the usefulness of this method in condensed-matter physics and materials science.

LOCK-IN THERMOGRAPHY METHOD

Because thermography can measure temperature distribution without contact, it is widely used, regardless of the industry or fundamental research. In recent years, a highly-sensitive temperature-distribution measurement method based on LIT was introduced for the operation and failure analyses of integrated circuits in the semiconductor industry [26]. In LIT, thermal images are measured using an infrared camera while the measurement object is periodically excited, and only the temperature change component following the excitation is extracted via Fourier analyses in real time. The temperature resolution that can be realistically achieved with conventional thermographic measurements is approximately 20–30 mK. In the LIT method, due to LIT's ability to accumulate thermal images for a long time, temperature resolution is improved; thus, highly-sensitive temperature-distribution measurements with a temperature resolution of <0.1 mK are possible. We applied the LIT method to the measurements of several thermoelectric, thermo-spin, and magnetocaloric phenomena that generate temperature changes by inputting a charge current, spin current, and magnetic field, respectively; consequently, we were able to elucidate properties and functions that were previously unknown.

As an example, we show a schematic of the LIT measurement for thermoelectric or thermo-spin effects in Fig. 2. Since a spin current is often generated from a charge current through spin-orbit interaction (e.g., the spin Hall effect [28-30]), the input is a charge current and the output is a temperature change induced by the thermoelectric or thermo-spin effects in this LIT measurement. Here, let us consider the case where a square-wave-modulated AC charge current with the frequency f and zero offset is applied to a sample. Because the thermoelectric or thermo-spin effect linearly responds to the input charge current, the temperature-change signals that vary with the same frequency f can be extracted through Fourier analyses of the obtained thermal images. In LIT, the thermal images are divided into an amplitude image that expresses the intensity distribution of the first harmonic component of the temperature change in response to the input signal and a phase image that expresses the phase-delay distribution of the temperature change (Fig. 2). The phase image indicates the time delay of the temperature change due to the thermal diffusion and also contains information on the sign of the temperature change. When the effect of thermal diffusion can be neglected, heating (cooling) corresponds to the case where the input charge current and output temperature change oscillate at the same (opposite) phase, which is defined as 0° (180°). Importantly, the Joule-heating background accompanying the zero-offset square-wave-modulated charge current is constant over time; thus, by extracting the first harmonic response via Fourier analyses, it is eliminated. Therefore, the LIT method allows for the pure and highly-sensitive detection of the thermoelectric or thermo-spin effects.

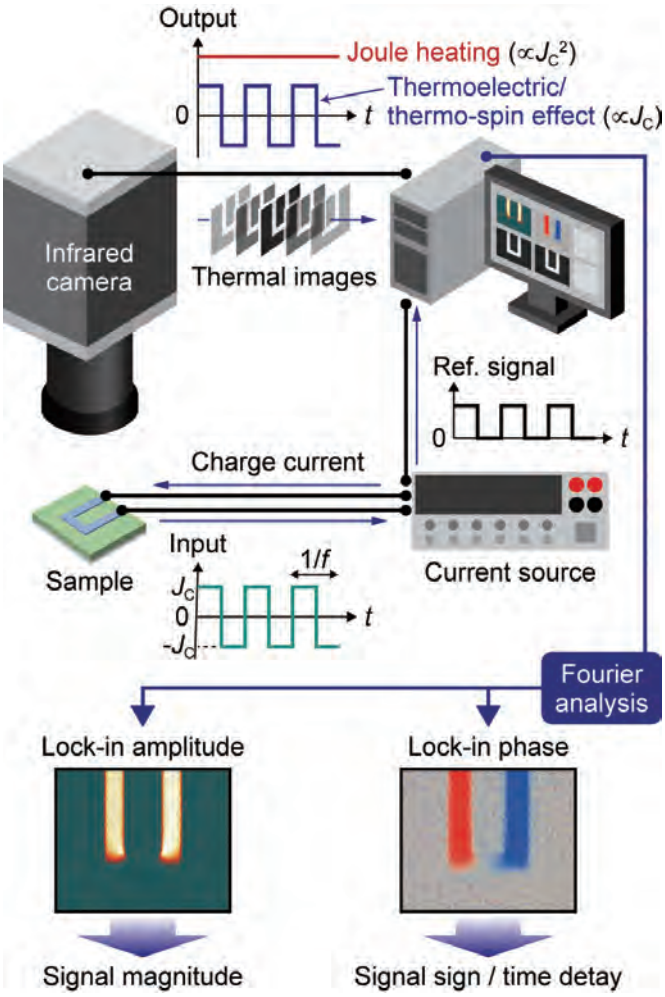

Fig. 2: Schematic of LIT measurement [12,16,17]. Thermal images are measured by an infrared camera and transferred to a processing system for extracting the first harmonic response of the temperature change induced by the periodically-oscillating input current.

The advantages of the LIT method are summarized as follows:

I. It can eliminate background, such as fluctuations in the ambient temperature, etc., that do not synchronize with the input-signal frequency.
II. By appropriately selecting the measurement condition and input-signal type, various thermal-response phenomena can be measured and evaluated.
III. It can obtain time information (thermal-diffusion information) from the phase delay.
IV. By increasing the lock-in frequency, the position of heat sources can be identified.

In general, LIT thermal images measured at low lock-in frequency show the temperature distribution nearly at steady states, while those at high frequency show the distribution at transient states, where the temperature broadening due to thermal diffusion is suppressed, providing the above advantage IV. In failure analyses of integrated circuits, by measuring the Joule heating concomitant with a charge current under a high lock-in frequency, the positions of the broken parts of the circuits are specified. Because depth information can also be obtained from the phase delay owing to thermal diffusion (as long as thermal diffusivity is known), non-destructive analyses of stacked devices can be realized without exposing electrode surfaces. In contrast, LIT also may be used for measurements of thermal diffusivity or thermal conductivity [31]. To apply the LIT method to spin-caloritronics research, our LIT system consists of not only standard components, such as an infrared camera, a lock-in input source (charge-current source), and an analysis system (personal computer), but we also have an electromagnet, which we put beneath the camera. By using the electromagnet, we can measure the magnetic-field dependence of temperature modulation. The imaging measurements of the SPE discussed below were performed using this system at room temperature and atmospheric pressure.

THERMAL IMAGING OF SPIN PELTIER EFFECT

A. Spin Peltier effect

The SPE is the reciprocal phenomenon of the SSE, in which a heat current is generated by a spin current. Experimental observation of the SPE was first reported by Flipse et al. [11] in 2014. They electrically detected the temperature change due to the spin injection that occured in a junction comprised of a ferrimagnetic insulator, yttrium iron garnet (YIG), and a Pt film, by using a thermopile temperature sensor prepared through microfabrication. The typical sample structure for measuring the SPE is a paramagnetic metal (PM) film with a large spin-orbit interaction formed on a ferrimagnetic insulator (FI). If a charge current $\mathbf{J}_C$ is applied to the PM film, the spin Hall effect generates a conduction-electron spin current $\mathbf{J}_S$ in the film thickness direction, generating spin accumulation polarized in the direction that satisfies the following relationship near the PM/FI interface [28-30]:

$$\mathbf{J}_S = -\frac{\hbar}{2e}\theta_{SH}\boldsymbol{\sigma}\times\mathbf{J}_C, \quad (1)$$

where e (>0), θ_{SH}, and $\boldsymbol{\sigma}$ are the elemental charge, spin Hall angle, and spin polarization vector, respectively. The generated spin accumulation is converted to a spin current carried by magnetization dynamics, i.e., magnons, in FI through an interfacial exchange interaction (Fig. 1). As a result of this spin-current transport and conversion, the spin-transfer torque [32] suppresses or enhances the precession amplitude of magnetic moments in FI depending on the direction of the spin current, which corresponds to the situation where the number of magnons is decreased or increased, respectively (Figs. 3(b) and 3(c)). Here,

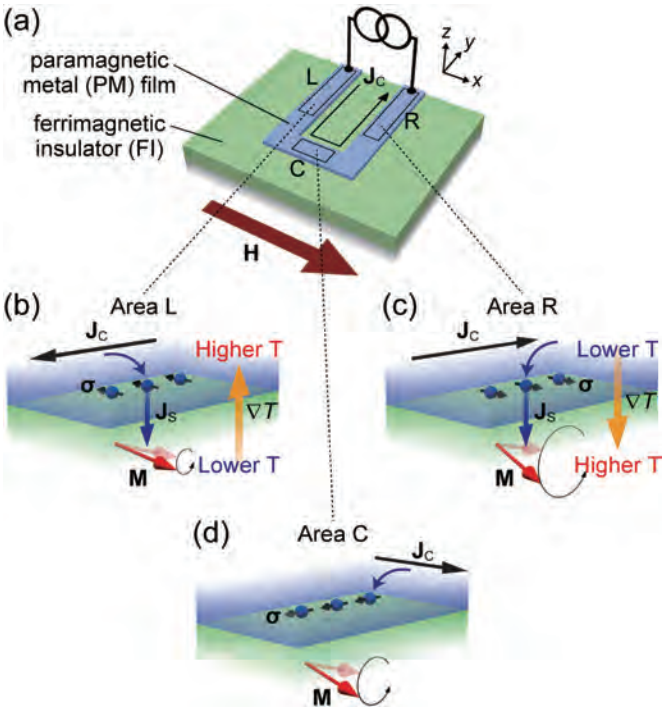

Fig. 3: (a) Schematic of the PM/FI sample used for measurements of the SPE [14]. The sample comprises a U-shaped PM (typically, Pt) film and an FI (typically, YIG). (b)-(d) Schematic illustrations of the SPE induced by the SHE [14] on areas L, R, and C. $\mathbf{J}_C$, $\mathbf{J}_S$, $\mathbf{M}$, and $\mathbf{H}$ denote the charge current applied to PM, spin current with the spin polarization vector $\boldsymbol{\sigma}$ generated by the spin Hall effect in PM, magnetization vector, and magnetic field vector, respectively. ∇T represents the temperature gradient appearing as a result of the SPE-induced heat current.

decreasing (increasing) the magnon number can be regarded as decreasing (increasing) magnon temperature. Because the magnon and lattice systems interact with each other, this spin-angular-momentum transfer induces a heat current across the PM/FI interface and changes the temperature near the interface with respect to the magnitude and direction of the spin current. Owing to a characteristic of spin-transfer torque, the direction of the heat current is dependent on whether the spin-polarization direction $\boldsymbol{\sigma}$ in PM is parallel or antiparallel to the magnetization $\mathbf{M}$ of FI. If $\boldsymbol{\sigma}$ is perpendicular to $\mathbf{M}$, a heat current is not generated (Fig. 3(d)). Consequently, the symmetry of the heat current $\mathbf{J}_Q$ generated by the SPE is expressed as

$$\mathbf{J}_Q \propto (\boldsymbol{\sigma}\cdot\mathbf{M})\mathbf{n} \propto \mathbf{J}_C \times \mathbf{M}, \qquad (2)$$

where $\mathbf{n}$ is the normal vector of the PM/FI interface [12,14].

B. Detection of temperature change induced by spin current

We realized the thermal imaging of the SPE by extracting the temperature change dependent on the spin polarization using the LIT method [12-14]. Figure 3(a) shows a schematic of the sample structure used in this study. A U-shaped Pt film is formed on the surface of a single-crystalline YIG substrate. By combining this structure with spatial information obtained from the imaging measurement, the symmetry of the SPE (Eq. (2)) can be verified. If the YIG layer is magnetized in the x direction, the direction of the spin polarization generated by the spin Hall effect becomes parallel or antiparallel to the magnetization in areas L and R; thus, temperature change due to the SPE appears. In contrast, in area C, these are perpendicular; thus, no temperature change is generated (Fig. 3(d)). Importantly, because the directions of the charge current and spin polarization in areas L are opposite to those in R, the direction of the SPE-induced heat current is reversed between these areas (Figs. 3(b) and (c)).

Figure 4 shows the results of the LIT measurements for the Pt/YIG sample. The LIT amplitude image in Fig. 4(a) clearly indicates that the current-induced temperature change appears in areas L and R, where the charge current is perpendicular to the magnetic field. In area C, where the current is parallel to the field, no temperature change is generated, which is consistent with Eq. (2). The temperature-change signals in areas L and R have phases that differ by 180°, indicating that the sign of the temperature change is reversed depending on the charge-current direction (Fig. 4(b)). The sign of the temperature change was also reversed by the reversal of the magnetic field (Figs. 4(c) and (d)). This behavior is clearly different from the temperature change due to Joule heating, which is independent of the direction of the charge current or the magnetic field.

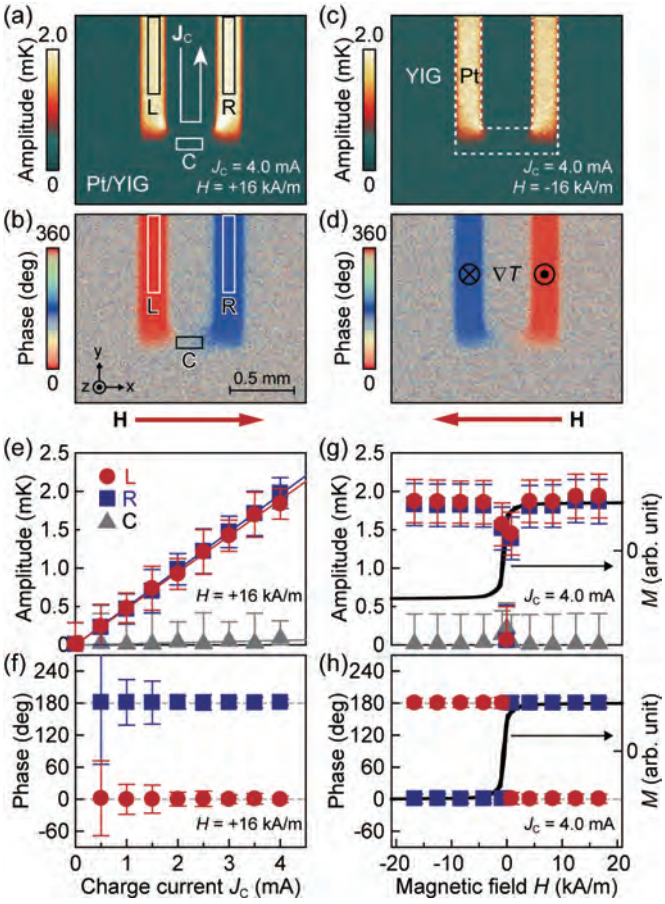

Fig. 4: (a),(b) Lock-in amplitude and phase images [12] for the Pt/YIG sample at the charge current amplitude of J_C = 4.0 mA and the magnetic field of H = +16 kA/m. (c),(d) Lock-in amplitude and phase images [12] for the Pt/YIG sample at J_C = 4.0 mA and H = -16 kA/m. (e),(f) J_C dependence of the lock-in amplitude and phase [12] on areas L (red circles), R (blue squares), and C (grey triangles) of the Pt/YIG sample at H = +16 kA/m. (g),(h) H dependence of the lock-in amplitude and phase [12] on L, R, and C of the Pt/YIG sample at J_C = 4.0 mA and the magnetization curve (black line) of the YIG.

To show that the observed signals originate from the SPE, we systematically measured the charge-current and magnetic-field dependence of the temperature change. Figures 4(e) and (f) respectively show the LIT amplitude and phase on areas L, R, and C for the Pt/YIG sample as a function of the charge-current amplitude. The magnitude of the temperature change increases in propor-

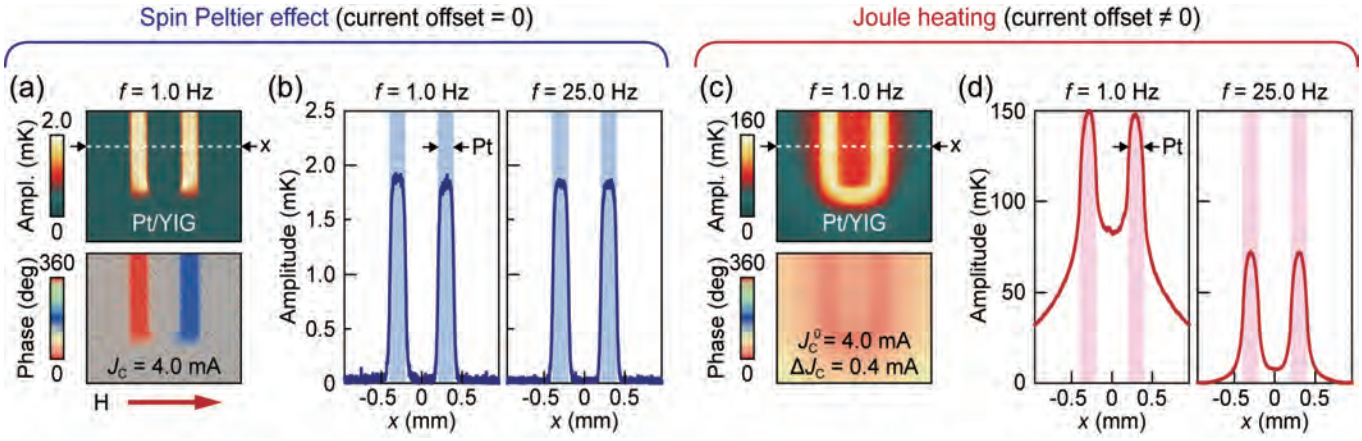

Fig. 5: (a) Lock-in amplitude and phase images [12] for the Pt/YIG sample at $J_C = 4.0$ mA, $H = +16$ kA/m, and $f = 1.0$ Hz, measured when the offset of the square-wave-modulated AC charge current is zero (SPE condition). (b) Lock-in amplitude profiles [12] along the x direction across areas L and R of the Pt/YIG sample at $J_C = 4.0$ mA, $H = +16$ kA/m, and $f = 1.0$ Hz or 25.0 Hz, measured in the SPE condition. (c) Lock-in amplitude and phase images [12] for the Pt/YIG sample at $H = 0$ kA/m and $f = 1.0$ Hz, measured when the offset and amplitude of the square-wave-modulated AC charge current is $J_C^0 = 4.0$ mA and $\Delta J_C = 0.4$ mA, respectively (Joule-heating condition). (d) Lock-in amplitude profiles [12] along the x direction across L and R of the Pt/YIG sample at $J_C^0 = 4.0$ mA, $\Delta J_C = 0.4$ mA, $H = 0$ kA/m, and $f = 1.0$ Hz or 25.0 Hz, measured in the Joule-heating condition.

tion to the current, while the phase difference between L and R remains 180°. This result is consistent with the characteristics of the SPE, which appears in linear response to the spin current injected in the YIG layer. It was confirmed that the magnetic-field dependence of the temperature-change signals corresponds to the magnetization process of the YIG layer (Fig. 4(g) and (h)). Furthermore, the sign of the temperature change was observed to be reversed when the Pt layer is replaced with a W film, where the sign of θ_{SH} of W is opposite to that of Pt [12,14]. By inserting a thin insulating film of Al_2O_3 that prevents the interaction of the spin accumulation and magnons between Pt and YIG, the temperature-change signal disappears. These results are consistent with Eqs. (1) and (2), supporting the interpretation that the observed temperature-change signal is attributed to the SPE. As shown here, by using the LIT method, the temperature modulation induced by a spin current can be visualized with high sensitivity.

C. Spatial distribution of temperature change and dipolar heat source

Figures 5(a) and (b) show the spatial distribution and profile along the x direction of the SPE-induced temperature change, respectively. Surprisingly, the temperature change was localized in the vicinity of the Pt/YIG junction where the spin current was injected. This result differs significantly from the temperature change due to standard heat sources, such as Joule heating, which is broadened from the heat-source positions through thermal diffusion (Figs. 5(c) and (d)). The spatial distribution of the Joule-heating-induced temperature change has strong lock-in frequency dependence, where the LIT images measured at low lock-in frequencies show a temperature distribution close to that at a steady state (Fig. 5(c)). In contrast, when the lock-in frequency increases, the temperature change is observed only near the heat-source positions (Fig. 5(d)). However, the temperature change induced by the SPE has completely different behavior and is not dependent on the lock-in frequency, at least in the range of 0.8–106.1 Hz (Fig. 5(b)) [16]. This experimental result indicates that the SPE signals reach the steady state in an extremely short time. These behaviors cannot be explained by single heat-source generation, showing the uniqueness of the heat source generated by the spin current.

In this study, we demonstrated that the unique temperature distribution accompanying the SPE is reproduced by assuming that the spin current generates a "dipolar heat source" near the PM/FI interface [12]. This dipolar heat source consists of an adjacent pair of a heat source and heat sink of equal magnitude. In contrast to a usual single heat source, the temperature change generated by a dipolar heat source is anisotropic (Figs. 6(a) and (b)). To explain the observed temperature distribution induced by the SPE in the PM/FI sample, we performed numerical simulations by means of a two-dimensional finite element method; here, we calculated the cross-sectional temperature distribution for a system where the dipolar

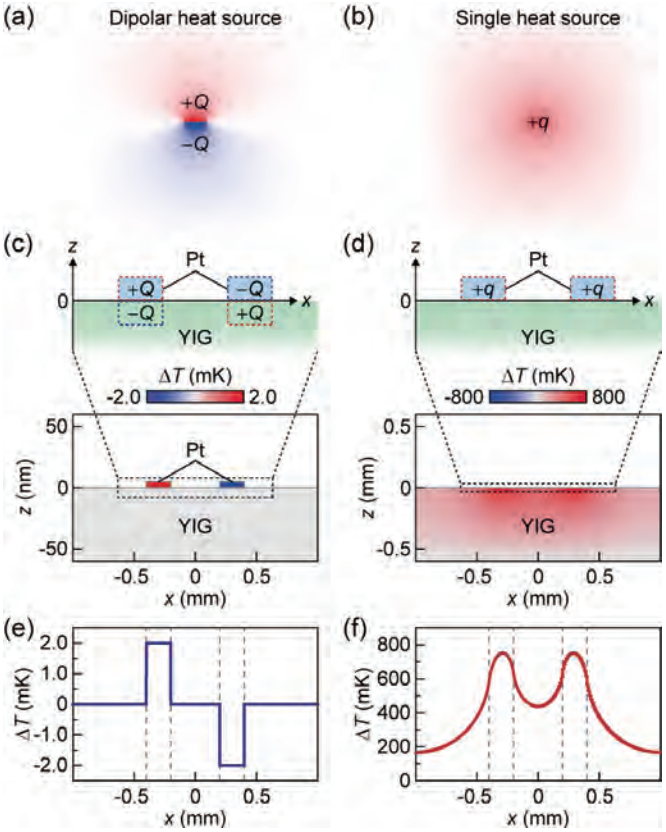

Fig. 6: (a),(b) Calculated temperature distributions [12] induced by a dipolar heat source comprised of a symmetric pair of a positive component $+Q$ and a negative component $-Q$ and a single heat source $+q$. The finite element calculations were performed by using COMSOL Multiphysics software. (c),(d) Calculated temperature difference ΔT distributions induced by dipolar heat sources on the Pt/YIG interfaces and the single heat sources on the Pt of the Pt/YIG model system (see Ref. [12] for details). The temperature of the bottom of the Pt/YIG system is fixed at 300 K and ΔT is defined as the difference from 300 K. (e),(f) ΔT profiles at the sample surface induced by the dipolar heat sources on the Pt/YIG interfaces and by the single heat sources on the Pt of the Pt/YIG system.

heat sources are set on the PM/FI interfaces. As shown in Figs. 6(c) and (e), the temperature distribution due to the dipolar heat sources is localized near the interfaces, consistent with the SPE experiments. For localized temperature change to occur, the magnitude of the heat sources and sinks must be exactly equal, and in this case, the net amount of heat is macroscopically zero; therefore, at a position away from the heat sources and sinks, no temperature change is generated. It is qualitatively interpreted that the dipolar heat-source generation due to a spin current is a consequence of the energy conservation in the conversion between the spin accumulation in PM and magnons in FI at the interface.

Localized heating and cooling effects accompanying the SPE were discovered through the imaging measurements based on the LIT method. In traditional studies where spatial distribution information could not be obtained, this unique temperature distribution was not taken into account in the analyses, and the amplitude of the temperature change was underestimated by more than one order of magnitude [11,12]. Presently, by redesigning an experimental setup considering the localized temperature distribution, the SPE-induced temperature change can be observed even with commercial thermocouple wires [15]. Systematic measurements and principle elucidation of the SPE are rapidly progressing, and recent years have seen developments in not only phenomenological model calculations [33,34] but also in microscopic theory [35].

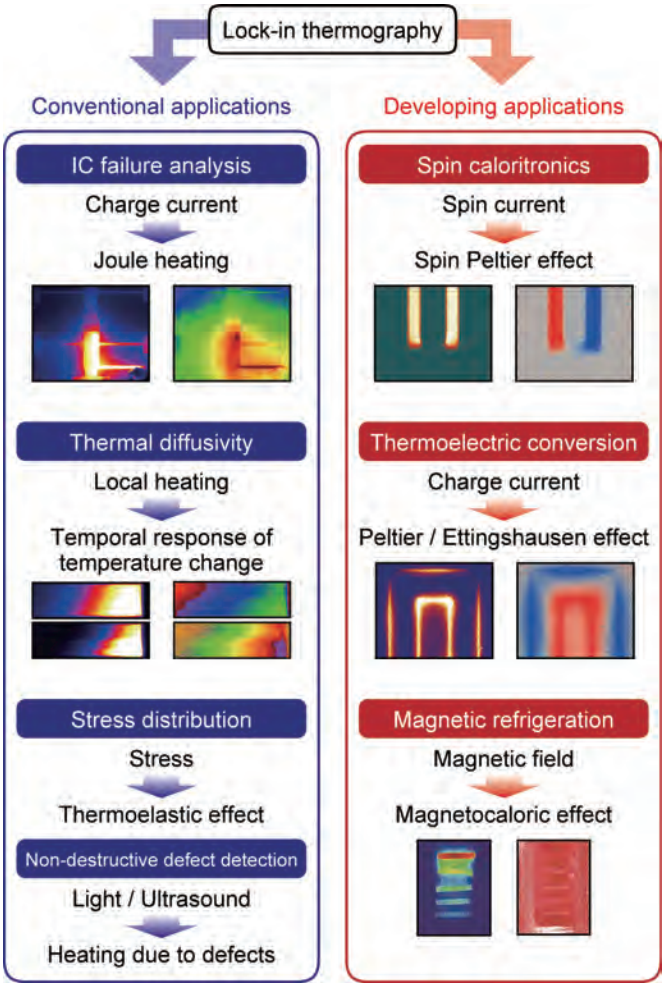

Fig. 7: Conventional and developing applications of the LIT method [17].

DEVELOPMENT OF SPIN CALORITRONICS USING LIT METHOD

In the aforementioned experiments, by using the periodic injection of the spin current as the lock-in input source, the imaging measurement of the SPE was achieved. However, the potential of the LIT method is not limited to SPE studies; it can be applied to various thermal-response phenomena by selecting the measurement condition and input-signal type. As shown in Fig. 7, we applied this method to spin-caloritronics studies from the viewpoints of both fundamental physics and materials science. Recently, the LIT method has allowed us to observe the anisotropic magneto-Peltier effect in a ferromagnetic metal [18], which had not been observed so far, and the anomalous Ettingshausen effect in a film [21]. The thermal imaging of such thermoelectric effects can be achieved through measurements similar to those performed in this study (Fig. 2). Furthermore, by extracting the temperature change induced by periodic magnetic fields using the LIT method, the magnetocaloric effect [24] can also be imaged. Importantly, the LIT method enables high-throughput measurements of adiabatic temperature change induced by the magnetocaloric effect, where measurement time can be significantly reduced in comparison to conventional methods. The fact that thermal-response properties of a large number of materials can be simultaneously evaluated and compared without increasing the measurement time is a major advantage in imaging measurements, and the LIT method is expected to contribute to the development of high-performance thermoelectric, thermo-spin, and magnetocaloric materials.

CONCLUSION

In this article, we introduced our recent works on spin caloritronics based on the LIT method, with a focus on the SPE. By using this method, temperature distribution can be resolved with high temperature and spatial resolutions, and thermal responses of spin-caloritronic phenomena can be investigated in a systematic and quantitative manner. An important point regarding the application of SPE clarified through the imaging measurements is the potential for actualizing local temperature control of spintronic devices. By using dipolar heat sources, one canrealize pinpoint temperature modulation without changing the surrounding temperature; this can lead to novel thermal management techniques. The temperature change generated by the SPE is presently small but can be increased by multi-layering PM/FI junctions [13]. In addition, materials exploration to improve the efficiency of the spin-to-heat current conversion is also dramatically developing [10]. We hope that the method proposed here paves the way for understanding detailed physics of spin-caloritronic phenomena, searching good materials, and creating new application technologies.

References

[1] K. Uchida, S. Takahashi, K. Harii, J. Ieda, W. Koshibae, K. Ando, S. Maekawa, and E. Saitoh: Nature 455, 778 (2008).
[2] K. Uchida, J. Xiao, H. Adachi, J. Ohe, S. Takahashi, J. Ieda, T. Ota, Y. Kajiwara, H. Umezawa, H. Kawai, G. E. W. Bauer, S. Maekawa, and E. Saitoh: Nat. Mater. 9, 894 (2010).
[3] C. M. Jaworski, J. Yang, S. Mack, D. D. Awschalom, J. P. Heremans, and R. C. Myers: Nat. Mater. 9, 898 (2010).
[4] K. Uchida, H. Adachi, T. Ota, H. Nakayama, S. Maekawa, and E. Saitoh: Appl. Phys. Lett. 97, 172505 (2010).
[5] S. Maekawa, E. Saitoh, S. O. Valenzuela, and T. Kimura (eds.): Spin Current (2nd edition) (Oxford University Press, 2017).
[6] G. E. W. Bauer, E. Saitoh, and B. J. van Wees: Nat. Mater. 11, 391 (2012).
[7] S. R. Boona, R. C. Myers, and J. P. Heremans: Energy Environ. Sci. 7, 885 (2014).
[8] M. Hatami, G. E. W. Bauer, Q. Zhang, and Paul J. Kelly: Phys. Rev. Lett. 99, 066603 (2007).
[9] A. Kirihara, K. Uchida, Y. Kajiwara, M. Ishida, Y. Nakamura, T. Manako, E. Saitoh, and S. Yorozu: Nat. Mater. 11, 686 (2012).
[10] K. Uchida, H. Adachi, T. Kikkawa, A. Kirihara, M. Ishida, S. Yorozu, S. Maekawa, and E. Saitoh: Proc. IEEE 104, 1946 (2016).
[11] J. Flipse, F. K. Dejene, D. Wagenaar, G. E. W. Bauer, J. B. Youssef, and B. J. van Wees: Phys. Rev. Lett. 113, 027601 (2014).
[12] S. Daimon, R. Iguchi, T. Hioki, E. Saitoh, and K. Uchida: Nat. Commun. 7, 13754 (2016).
[13] K. Uchida, R. Iguchi, S. Daimon, R. Ramos, A. Anadón, I. Lucas, P. A. Algarabel, L. Morellón, M. H. Aguirre, M. R. Ibarra, and E. Saitoh: Phys. Rev. B 95, 184437 (2017).
[14] S. Daimon, K. Uchida, R. Iguchi, T. Hioki, and E. Saitoh: Phys. Rev. B 96, 024424 (2017).
[15] R. Itoh, R. Iguchi, S. Daimon, K. Oyanagi, K. Uchida, and E. Saitoh: Phys. Rev. B 96, 184422 (2017).
[16] R. Iguchi and K. Uchida: Jpn. J. Appl. Phys. 57, 0902B6 (2018).
[17] K. Uchida: OYO BUTURI 87, 506-510 (2018).
[18] K. Uchida, S. Daimon, R. Iguchi, and E. Saitoh: Nature 558, 95 (2018).
[19] P. W. Bridgman: Phys. Rev. 24, 644 (1924).
[20] E. H. Hall: Phys. Rev. 26, 820 (1925).
[21] T. Seki, R. Iguchi, K. Takanashi, and K. Uchida: Appl. Phys. Lett. 112, 152403 (2018).
[22] P. Weiss and A. Piccard: J. Phys. Theor. Appl. 7, 103 (1917).
[23] A. M. Tishin, in Handbook of Magnetic Materials, edited by K. H. J. Buschow (North Holland) 12, 395 (1999).
[24] Y. Hirayama, R. Iguchi, X.-F. Miao, K. Hono, and K. Uchida: Appl. Phys. Lett. 111, 163901 (2017).
[25] H. Straube, J.-M. Wagner, and O. Breitenstein: Appl. Phys. Lett. 95, 052107 (2009).

[26] O. Breitenstein, W. Warta, and M. Langenkamp: Lock-in Thermography Basics and Use for Evaluating Electronic Devices and Materials (Springer Science & Business Media, 2010).
[27] O. Wid, J. Bauer, A. Müller, O. Breitenstein, S. S. P. Parkin, and G. Schmidt: Sci. Rep. 6, 28233 (2016).
[28] Y. K. Kato, R. C. Myers, A. C. Gossard, and D. D. Awschalom: Science 306, 1910 (2004).
[29] J. Wunderlich, B. Kaestner, J. Sinova, and T. Jungwirth: Phys. Rev. Lett. 94, 047204 (2005).
[30] J. Sinova, S. O. Valenzuela, J. Wunderlich, C. H. Back, and T. Jungwirth: Rev. Mod. Phys. 87, 1213 (2015).
[31] T. Ishizaki and H. Nagano: Int. J. Thermophys. 36, 2577 (2015).
[32] Y. Tserkovnyak, A. Brataas, G. E. W. Bauer, and B. I. Halperin: Rev. Mod. Phys. 77, 1375 (2005).
[33] V. Basso, E. Ferraro, A. Magni, A. Sola, M. Kuepferling, and M. Pasquale: Phys. Rev. B 93, 184421 (2016).
[34] L. J. Cornelissen, K. J. H. Peters, G. E. W. Bauer, R. A. Duine, and B. J. van Wees: Phys. Rev. B 94, 014412 (2016).
[35] Y. Ohnuma, M. Matsuo, and S. Maekawa: Phys. Rev. B 96, 134412 (2017).

Ken-ichi Uchida has been a group leader of the Spin Caloritronics Group at the Research Center for Magnetic and Spintronic Materials, National Institute for Materials Science in Japan, since 2016. After receiving a PhD from Tohoku University, Sendai, Japan, he worked at the Institute for Materials Research, Tohoku University as an assistant professor (2012-2014) and an associate professor (2014-2016). His research fields are spintronics and spin caloritronics.